Channel Modeling and and Parameter Optimization for Hovering UAV-Based Free-Space Optical Links

Mohammad Taghi Dabiri, Seyed Mohammad Sajad Sadough, Mohammad Ali Khalighi

Channel Modeling and Parameter Optimization for Hovering UAV-Based Free-Space Optical Links

M.T. Dabiri, S.M.S. Sadough and M.A. Khalighi

***Abstract*—Recently, the use of multi-rotor (MR) unmanned aerial vehicles (UAVs) has emerged as a promising solution for establishing flexible free-space optical (FSO) communication links. We address in this paper accurate channel modeling to assess the benefits of MR UAV-based deployment for such links. In particular, in the absence of active tracking subsystems, we derive statistical models for ground-to-UAV, UAV-to-UAV, and UAV-to-ground links over both Gamma-Gamma and log-normal atmospheric turbulence models. Unlike previous works on this topic, our proposed model considers the joint effect of atmospheric turbulence along with position and angle-of-arrival fluctuations. The high accuracy of the proposed analytical models is verified by comparing numerically solved and Monte-Carlo simulation results in terms of link outage probability. We further discuss the impact of different transmitter/receiver parameters and their optimization in view of maximizing the link availability.**

***Index Terms*—Free-space optics; unmanned aerial vehicles; angle-of-arrival fluctuations; atmospheric turbulence.**

I. Introduction

DUE to the relatively high cost of deploying optical fibers, and the spectrum congestion that radio frequency systems are increasingly facing with, free-space optical (FSO) communications have recently attracted a growing attention as a cost-effective alternative technology for high data-rate point-to-point transmission in a wide range of applications [1]–[3]. Nevertheless, the performance of FSO links is impaired by several factors including geometric and atmospheric loss, and atmospheric turbulence, which are all distance-dependent. Also, there is a stringent line-of-sight (LOS) requirement between the transmitter (Tx) and the receiver (Rx) due to the typically narrow beams used [4]. Here, relay nodes can be inserted between the Tx and the Rx to improve link reliability an performance [5]. However, relay placement in optimal locations is not always possible, and particular attention should be devoted to the risk of exposure at rental relay locations. Recently, the use of unmanned aerial vehicles (UAV) has emerged as a promising solution [6]; but establishing such links of high reliability appeals for a number of challenges, including the necessity of precise link alignment [7].

Establishing aerial FSO links has been an important topic of research in the past. Initial works concerned laser communication for inter-satellite and satellite-to-ground links [1]. More recently, high-altitude platform (HAP)-based FSO networks have received a great deal of attention [8]–[10]. Multi-rotor (MR) UAVs are an attractive option in relatively shorter links due to their advantages of high maneuverability, small size and low cost. They are increasingly employed in several applications, serving as mobile aerial base stations to enhance wireless connectivity [11]. There are, however, basic differences between satellite/HAP-based and MR UAV-based systems, especially, regarding the characteristics of the communication channel [12], which require dedicated study of the impact of different link parameters on the overall performance.

The literature on UAV-based FSO communications is relatively recent. In [6], experimental demonstration of a 100 m-roundtrip 80-Gbps orbital-angular-momentum-based FSO link was presented between a UAV and a ground station. In [13], the use of flying platforms was proposed for backhaul/fronthaul connectivity of cellular networks via FSO/milimeter-wave links. The benefits of deploying UAVs for relay-assisted FSO systems were investigated in [14]. A channel model was introduced in [15] for an FSO link between a UAV and a ground robot. Also, a tracking scheme for automatic alignment between mobile nodes was proposed in [16]. Open loop link alignment modeling was considered in [17] for an FSO link between two hovering UAVs.

To assess the benefits of UAV deployment for FSO communications, one important aspect is accurate channel modeling, which has been the subject of a few recent works. Most of these do not consider the effect of atmospheric turbulence that can severely affect the link performance. Another important factor is angle-of-arrival (AOA) fluctuations due to orientation deviations of hovering MR UAVs [12]. Indeed, for FSO links between fixed platforms, wind and thermal expansions result in random fluctuations in the aperture position and orientation, where the former parameter has the dominant effect [18]. For UAV-based links, however, the effect of AOA fluctuations should not be neglected. A recent work [19], considered channel modeling including the effects of AOA fluctuations, turbulence, and Tx/Rx position fluctuations. There, to simplify the analytical derivations, the effect of Tx vibrations on AOA fluctuations was neglected by making far-field assumptions. Moreover, the results of [19] are obtained for log-normal turbulence whose validity is limited to the weak turbulence regime.

In this paper, assuming the absence of active tracking subsystems, we model a MR UAV-based FSO link in the presence of atmospheric turbulence by considering both position and AOA fluctuations. As illustrated in Fig. 1, a general MR UAV-based link can be divided into three different links: ground-to-UAV (GU), UAV-to-UAV (UU) and UAV-to-ground (UG).

M. T. Dabiri and S. M. S. Sadough are with the Department of Electrical Engineering, Shahid Beheshti University G. C., 1983969411, Tehran (e-mail: s_sadough@sbu.ac.ir).

M. A. Khalighi is with the Aix Marseille University, CNRS, Centrale Marseille, Institut Fresnel, Marseille, France (e-mail: Ali.Khalighi@fresnel.fr).

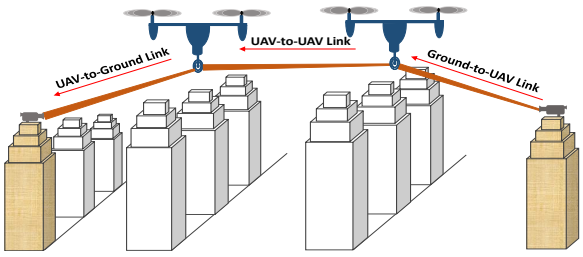

Fig. 1. Illustration of a typical MR UAV-based FSO communication link.

Our performance evaluation is mainly based on the outage probability, which is the most relevant metric for quasi-static FSO channels. As we will show later, each channel depends on nine random variables (RVs). We provide closed-form expressions for the probability density function (PDF) of the three link types, as well as analytical expressions for the outage probability over both Gamma-Gamma (GG) and log-normal (LN) atmospheric turbulence models, which require only one-dimensional integration. Moreover, we provide a detailed and insightful analysis of the parameter optimization of the Tx/Rx such as the Tx beam-width and the Rx field-of-view (FOV) that can be quite useful for the practical design of these links. In Section II, we describe our system model and main assumptions. Analytical formulations of the channel PDF for the MR UAV-based links are developed then in Section III. Next, Section IV presents numerical results to show the accuracy of the proposed models as well as to study the link performance and parameter optimization. Lastly, in Section V, we present our main conclusions and a few future research directions.

II. System Model and Main Assumptions

Figure 2 illustrates the 2-D schematic diagram of a UU system consisting of two hovering UAVs. To model the UU link parameters in 3-D space, we make the following assumptions:

- the two highly stable aerial nodes hover in one place;
- in the Cartesian coordinate system $[x, y, z] \in \mathbb{R}^{1\times 3}$, the mean positions of the Tx and Rx are at $A_{T_x} = [0, 0, 0]$ and $A_{R_x} = [0, 0, Z]$, respectively, and are perfectly known to Tx/Rx, which can be realized through periodic data exchange between them;
- the mean orientation vectors of the Tx and the Rx are located on the z axis;
- instantaneous position and orientation of the Tx and the Rx are slightly deviated from their means under the effect of numerous random events related to UAV hovering;
- no spatial or temporal tracking is done.

Within the Cartesian coordinates, RVs A'_{T_x}=$[x_t, y_t, z_t]$ and A'_{R_x}=$[x_r, y_r, Z$+$z_r]$ denote the instantaneous positions of the Tx and the Rx nodes, respectively, with respect to their mean A'_{T_x} and A'_{R_x}. We assume that x_t, x_r, y_t, y_r, z_t and z_r are very small, compared with the link range Z. Then, angles φ_{tx}, φ_{ty}, φ_{rx} and φ_{ry}, indicated in Fig. 2, can be approximated as: $\varphi_{tx} \simeq \frac{x_t}{Z}$, $\varphi_{ty} \simeq \frac{y_t}{Z}$, $\varphi_{rx} \simeq \frac{x_r}{Z}$ and $\varphi_{ry} \simeq \frac{y_r}{Z}$.

In addition to the random displacements, the optical axes of the Tx and Rx also vary randomly. In $[x, z]$ and $[y, z]$ Cartesian coordinates, we denote the instantaneous Tx and Rx misalignment orientations by θ_{tx}, θ_{ty}, θ_{rx} and θ_{ry}, respectively.

We consider highly stable hovering MR UAVs which offer high angular stability on the order of mrad thanks to the accuracy of mechanical and control systems. Thus, assuming that θ_{tx} and θ_{ty} are sufficiently small, we can use small-angle approximation as follows.

$$\begin{aligned} x_{\theta_{tx}} &= \tan(\theta_{tx})\, Z \simeq \theta_{tx} Z, \\ y_{\theta_{ty}} &= \tan(\theta_{ty})\, Z \simeq \theta_{ty} Z, \end{aligned} \tag{1}$$

where $x_{\theta_{tx}}$ and $y_{\theta_{ty}}$ denote the beam position deviations at the Rx, respectively. Based on the central limit theorem, position and orientation deviations are considered as Gaussian distributed as they result from numerous random events [12]. We assume that the variances of position deviations are the same in x, y and z axes. Therefore, considering the same conditions for the two hovering MR UAVs, x_t, x_r, y_t, y_r, z_t and z_r are modeled as zero-mean independent Gaussian RVs with variance σ_p^2, and θ_{tx}, θ_{ty}, θ_{rx} and θ_{ry} are modeled as zero-mean independent Gaussian RVs with variance σ_θ^2.

A. Received Signal Model

Typically a converging lens is used before the photo-detector (PD), which converts the received intensity to a photo-current. The Rx also collects undesired background radiations due mainly to scattered sunlight [20], [21]. Subtracting a constant bias due to the background noise mean power, the PD output corresponding to the kth symbol interval, i.e., $[(k-1)T_b, kT_b)$ with T_b being the symbol duration, can be written as [22]

$$r[k] = R\, h\, s[k] + n[k], \tag{2}$$

where h denotes the channel attenuation coefficient, $n[k]$ is the photo-current noise, $s[k]$ is the transmitted symbol with average optical power P_t, and R is the PD responsitivity. We assume that the background noise is the dominant noise source at the Rx and consider $n[k]$ as a signal-independent zero-mean Gaussian noise with variance $\sigma_n^2 = 2e\, B_e\, R\, P_b$, where e denotes the electron charge and B_e is the PD bandwidth (in Hz). Furthermore, P_b denotes the background power, which can be formulated as $P_b = N_b(\lambda)\, B_o\, \Omega_{FOV}\, A_a$, where $N_b(\lambda)$ is the spectral radiance of the background radiations at wavelength λ (in Watts/cm^2-μm-srad), B_o is the bandwidth of the optical filter at the Rx (in μm) and A_a is the lens area (in cm^2) [23, Eq. (3b)]. Moreover, Ω_{FOV} denotes the Rx's FOV (in srad) that can be obtained as $\Omega_{FOV} = 2\pi\big(1 - \cos(\theta_{FOV}/2)\big) \simeq \pi\, \theta_{FOV}^2/4$. The instantaneous electrical signal-to-noise ratio (SNR) is defined as $\Upsilon = R^2 P_t^2 h^2/\sigma_n^2$. In slow fading channels, which is typical of FSO links, the outage probability $\mathcal{P}_{\text{out}}$ (i.e., the probability that the instantaneous SNR falls below a threshold Υ_{th}) is the most appropriate performance metric. We define $\mathcal{P}_{\text{out}}$ as

$$\mathcal{P}_{\text{out}} = \int_0^{\Upsilon_{th}} f_\Upsilon(\Upsilon)\, d\Upsilon = \int_0^{h_{th}} f_h(h) dh, \tag{3}$$

where

$$h_{th} = \sqrt{\sigma_n^2 \Upsilon_{th}}\,/RP_t, \tag{4}$$

and f_Υ and f_h denote the PDFs of Υ and h, respectively.

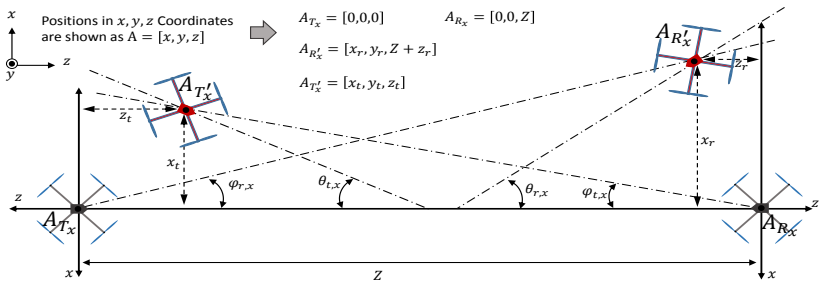

Fig. 2. Schematic 2-D diagram of a UU system consisting of two hovering MR UAV nodes. A_{T_x} and A_{R_x} are the mean of Tx and Rx positions, and A'_{T_x} and A'_{R_x} show the deviations from A_{T_x} and A_{R_x}, respectively.

III. Channel Modeling

The considered source-to-destination link involves three different channels, i.e., GU, UU, and UG, see Fig. 1. We first develop the channel model for the UU link, based on which we later provide the model for the GU and UG channels.

A. UAV-to-UAV Channel Modeling

Our model takes into account four impairments, i.e., the atmospheric attenuation h_l, the atmospheric turbulence h_a, the pointing error loss h_{pg}, and the link interruption h_{pa} due to the AOA fluctuations. The UU channel coefficient is then,

$$h = h_l\, h_a\, h_{pg}\, h_{pa}. \tag{5}$$

1) Atmospheric Attenuation and Turbulence: The atmospheric attenuation is typically modeled by the Beer-Lambert law as $h_l = \exp(-Z\xi)$, with ξ being the scattering coefficient, which is a function of visibility [2]. Considering the atmospheric turbulence induced fading, we use LN and GG models; the former is appropriate for weak turbulence conditions whereas the latter can describe all turbulence regimes [2], [24]. The distribution of h_a according to the LN model is

$$f_{\mathrm{L}}(h_a) = \frac{1}{2h_a\sigma_{\mathrm{Ln}h_a}\sqrt{2\pi}} \exp\left(-\frac{\left(\ln(h_a) - 2\mu_{\mathrm{Ln}h_a}\right)^2}{8\sigma^2_{\mathrm{Ln}h_a}}\right). \tag{6}$$

where $\mu_{\mathrm{Ln}h_a}$ and $\sigma^2_{\mathrm{Ln}h_a}$ denote the mean and variance of log-irradiance, respectively, where $\sigma^2_{\mathrm{Ln}h_a} \simeq \sigma^2_R/4$ with σ^2_R being the Rytov variance [25]. Setting $\mathbb{E}[h_a] = 1$ (with $\mathbb{E}[.]$ denoting the expected value) we have $\mu_{\mathrm{Ln}h_a} = -\sigma^2_{\mathrm{Ln}h_a}$.

For the GG model, the distribution of the random variable h_a is given by [24]

$$f_{\mathrm{G}}(h_a) = \frac{2(\alpha\beta)^{\frac{\alpha+\beta}{2}}}{\Gamma(\alpha)\Gamma(\beta)} h_a^{\frac{\alpha+\beta}{2}-1} k_{\alpha-\beta}(2\sqrt{\alpha\beta h_a}), \tag{7}$$

where $\Gamma(.)$ is the Gamma function and $k_n(.)$ is the modified Bessel function of the second kind of order n. Also, α and β are respectively the effective number of large-scale and small-scale eddies, which depend on Rytov variance σ^2_R [24]. Unless otherwise mentioned, we consider the GG channel model in the following.

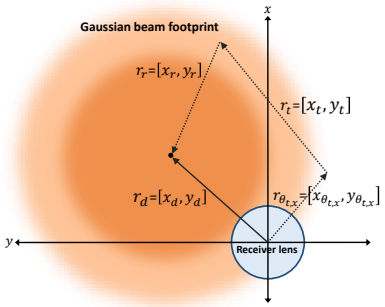

Fig. 3. Gaussian beam footprint at the Rx aperture. The center of received beam is deviated from the center of Rx lens due to the random displacement of hovering Tx and Rx and also due to the orientation deviation of Tx.

2) Pointing Error Loss: We consider a Gaussian beam at the Tx, for which the normalized spatial distribution of the transmitted intensity at distance Z, is given by [24]

$$I_r(r, Z) = \frac{2}{\pi w_z} \exp\left(-\frac{2(x^2+y^2)}{w_z^2}\right), \tag{8}$$

where $r = [x, y]$ is the radial distance vector from the beam center and w_z is the beam waist at distance Z. Let us consider the beam spot as shifted to the position $r_d = [x_d, y_d]$ with respect to the center of the Rx lens, as depicted in Fig. 3. The RVs x_d and y_d are obtained as

$$x_d = x_{tr} + Z\theta_{tx}, \quad \text{and} \quad y_d = y_{tr} + Z\theta_{ty}, \tag{9}$$

where $x_{tr} = x_t + x_r$ and $y_{tr} = y_t + y_r$ are zero mean Gaussian RVs with variance $2\sigma_p^2$. Considering the Rx lens radius r_a, the pointing error loss h_{pg} (which includes the geometric loss as well) can be expressed as

$$h_{pg} = \int_{-r_a}^{r_a} \int_{-\sqrt{r_a^2-y^2}}^{\sqrt{r_a^2-y^2}} \frac{2}{\pi w_z} \times \exp\left(-2\frac{(x+x_d)^2 + (y+y_d)^2}{w_z^2}\right) dxdy. \tag{10}$$

Using [18, Eqs. (8), (9)], (10) can be approximated as

$$h_{pg} \simeq A_0 \exp\left(-2r_{tr}^2/w_{z_{\mathrm{eq}}}^2\right), \tag{11}$$

where $r_{tr} = \sqrt{x_d^2 + y_d^2}$. The parameter $A_0 = (\mathrm{erf}(\nu))^2$ denotes the maximal fraction of the collected intensity with

$\nu = \frac{\sqrt{\pi} r_a}{\sqrt{2} w_z}$, $w_{z_{\rm eq}}^2 = w_z^2 \frac{\sqrt{\pi}\mathrm{erf}(\nu)}{2\nu \exp(-\nu^2)}$ is the equivalent beam waist, and $\mathrm{erf}(.)$ is the error function. Since the RVs x_d and y_d conditioned on θ_{tx} and θ_{ty}, respectively, have a Gaussian distribution as $x_d \sim \mathcal{N}(\theta_{tx} Z, 2\sigma_p^2)$ and $y_d \sim \mathcal{N}(\theta_{ty} Z, 2\sigma_p^2)$, r_{tr} conditioned on θ_{tx} and θ_{ty} has a Rician distribution as

$$f_{r_{tr}|\theta_{xy}}(r_{tr}) = \frac{r_{tr}}{2\sigma_p^2} \exp\left(-\frac{r_{tr}^2 + \theta_{xy}^2 Z^2}{4\sigma_p^2}\right) I_0\left(\frac{Z\theta_{xy} r_{tr}}{2\sigma_p^2}\right). \quad (12)$$

$I_0(.)$ is the modified Bessel function of the first kind with order zero, and $\theta_{xy} = \sqrt{\theta_{tx}^2 + \theta_{ty}^2}$ is Rayleigh distributed as:

$$f_{\theta_{xy}}(\theta_{xy}) = \left(\theta_{xy}/\sigma_\theta^2\right) \times \exp\left(-\theta_{xy}^2/2\sigma_\theta^2\right). \quad (13)$$

According to (11) and (12) and after some algebra, the PDF of h_{pg} conditioned on θ_{xy} is derived as

$$\begin{aligned} f_{h_{pg}|\theta_{xy}}(h_{pg}) =& \frac{w_{z_{eq}}^2}{4h_{pg}\sqrt{-\frac{w_{z_{eq}}^2}{2}\ln\left(\frac{h_{pg}}{A_0}\right)}} \\ & \times f_{r_{tr}|\theta_{xy}}\left(\sqrt{-\frac{w_{z_{eq}}^2}{2}\ln\left(\frac{h_{pg}}{A_0}\right)}\right) \\ =& \frac{w_{z_{eq}}^2}{8A_0\sigma_p^2} \exp\left(-\frac{\theta_{xy}^2 Z^2}{4\sigma_p^2}\right) \left(\frac{h_{pg}}{A_0}\right)^{\frac{w_{z_{eq}}^2}{8\sigma_p^2}-1} \\ & \times I_0\left(\frac{Z\theta_{xy}}{2\sigma_p^2}\sqrt{-\frac{w_{z_{eq}}^2}{2}\ln\left(\frac{h_{pg}}{A_0}\right)}\right), \\ & \text{for} \quad 0 \le h_{pg} \le A_0. \end{aligned} \quad (14)$$

Considering the GG turbulence model, from (7), (13) and (14), the distribution of $h' = h_l h_a h_{pg}$ conditioned on θ_{xy} is obtained as

$$\begin{aligned} f_{h'|\theta_{xy}}^{\rm G}(h') =& \int_0^\infty f_{h'|h_a,\theta_{xy}}(h') f_{h_a}(h_a) dh_a \\ =& \int_0^\infty \frac{1}{h_a h_l} f_{h_{pg}|\theta_{xy}}\left(\frac{h'}{h_a h_l}\right) f_{h_a}(h_a) dh_a \quad (15) \\ =& \frac{2(\alpha\beta)^{\frac{\alpha+\beta}{2}}}{\Gamma(\alpha)\Gamma(\beta)} \frac{\gamma_{uu}^2 h'^{\gamma_{uu}^2-1}}{(A_0 h_l)^{\gamma_{uu}^2}} \exp\left(-\frac{\theta_{xy}^2 Z^2}{4\sigma_p^2}\right) \\ & \times \int_{\frac{h'}{A_0 h_l}}^\infty I_0\left(\frac{Z\theta_{xy}}{2\sigma_p^2}\sqrt{-\frac{w_{z_{eq}}^2}{2}\ln\left(\frac{h'}{A_0 h_l h_a}\right)}\right) \\ & \times h_a^{\frac{\alpha+\beta}{2}-\gamma_{uu}-1} k_{\alpha-\beta}(2\sqrt{\alpha\beta h_a}) dh_a. \quad (16) \end{aligned}$$

where $\gamma_{uu}^2 = w_{z_{eq}}^2/8\sigma_p^2$. Using [26, Eq. (03.04.06.0002.01)], the modified Bessel function of the second kind $k_\nu(x)$ can be approximated as

$$k_\nu(x) = \frac{\pi}{2\sin(\pi\nu)} \sum_{n=0}^\infty \left[\frac{(x/2)^{2n-\nu}}{\Gamma(n-\nu+1)n!} - \frac{(x/2)^{2n+\nu}}{\Gamma(n+\nu+1)n!}\right]. \quad (17)$$

Applying a change of variable $z = \sqrt{-\frac{w_{z_{eq}}^2}{2}\ln\left(\frac{h'}{A_0 h_l h_a}\right)}$ and using (17), (62), [27, Eqs. (6.643.2) and (9.227)], after some manipulations, a closed form expressions for (16) is derived as

$$\begin{aligned} f_{h'|\theta_{xy}}^{\rm G}(h') \simeq & \sum_{j=0}^J \Big(\mathcal{A}_j(\alpha,\beta) e^{-a_j\theta_{xy}^2} h'^{\beta-1+j} \\ & - \mathcal{A}_j(\beta,\alpha) e^{-b_j\theta_{xy}^2} h'^{\alpha-1+j}\Big), \end{aligned} \quad (18)$$

where

$$\mathcal{A}_j(\alpha,\beta) = \frac{\pi\gamma_{uu}^2 \left(\frac{\alpha\beta}{A_0 h_l}\right)^\beta \sin^{-1}((\alpha-\beta)\pi)}{\Gamma(\alpha)\Gamma(\beta)\Gamma(-(\alpha-\beta)+1)|-(\beta-\gamma_{uu}^2)|},$$

and $a_j = \frac{Z^2}{4\sigma_p^2} + \frac{Z^2\gamma_{uu}^2}{4\sigma_p^2(\beta-\gamma_{uu}^2+j)}$, $b_j = \frac{Z^2}{4\sigma_p^2} + \frac{Z^2\gamma_{uu}^2}{4\sigma_p^2(\alpha-\gamma_{uu}^2+j)}$ and $J = \lfloor \gamma_{uu}^2 - \alpha \rfloor$.

3) Link Interruption due to AOA Fluctuations: Let us define the AOA of the signal as the incidence angle relative to the Rx axis that we denote by θ_a. According to (1), θ_a can be closely approximated as

$$\theta_a \simeq \sqrt{(\theta_{tx}+\theta_{rx})^2 + (\theta_{ty}+\theta_{ry})^2}. \quad (19)$$

Given the limited Rx FOV, a link interruption occurs for $\theta_a > \theta_{FOV}$. Thus the corresponding loss h_{pa} due to AOA fluctuations can be written as

$$h_{pa} = \Pi\left(\theta_a/\theta_{FOV}\right), \quad (20)$$

where $\Pi(x) = 1$ if $|x| \le 1$, and $\Pi(x) = 0$ otherwise.

4) Overall Channel Model: According to link interruption formulation in (19), (20) and after some derivations provided in Appendix A, we obtain the distribution of h conditioned on θ_{xy} as

$$\begin{aligned} f_{h|\theta_{xy}}(h) =& F_{\theta_a|\theta_{xy}}(\theta_{FOV}) f_{h'|\theta_{xy}}(h) \\ & + \left(1 - F_{\theta_a|\theta_{xy}}(\theta_{FOV})\right)\delta(h), \end{aligned} \quad (21)$$

where

$$F_{\theta_a|\theta_{xy}}(\theta_{FOV}) \simeq 1 - \exp\left(-\frac{\theta_{xy}^2}{2\sigma_\theta^2}\right) \sum_{m=0}^M \mathcal{H}(m) \left(\frac{\theta_{xy}^2}{\sigma_\theta^2}\right)^m, \quad (22)$$

and $\delta(.)$ is Dirac delta function [27] and $\mathcal{H}(m)$ is defined in (46). Lastly, the PDF of h can be obtained as

$$f_h(h) = \int_0^\infty f_{h|\theta_{xy}}(h) f_{\theta_{xy}}(\theta_{xy}) d\theta_{xy}. \quad (23)$$

Substituting (13), (18), (21) and (22) in (23), we obtain the PDF of h for UU link as

$$f_G^{uu}(h) = f_G^{uu}(h>0) + f_G^{uu}(h=0)\delta(h), \quad (24)$$

where $f_G^{uu}(h>0)$ is expressed as

$$\begin{aligned} & f_G^{uu}(h>0) \simeq \\ & \sum_{j=0}^J \int_0^\infty \frac{\theta_{xy}}{\sigma_\theta^2} \left(1 - \exp\left(-\frac{\theta_{xy}^2}{2\sigma_\theta^2}\right) \sum_{m=0}^M \mathcal{H}(m) \left(\frac{\theta_{xy}^2}{\sigma_\theta^2}\right)^m\right) \\ & \times \left(\mathcal{A}_j(\alpha,\beta) \exp\left(-\left(a_j + \frac{1}{2\sigma_\theta^2}\right)\theta_{xy}^2\right) h^{\beta-1+j} \right. \\ & \left. - \mathcal{A}_j(\beta,\alpha) \exp\left(-\left(b_j + \frac{1}{2\sigma_\theta^2}\right)\theta_{xy}^2\right) h^{\alpha-1+j}\right) d\theta_{xy}. \end{aligned} \quad (25)$$

Also, by using [27, Eq. (3.461.3)], a closed-form expression for $f_G^{uu}(h=0)$ can be derived as

$$f_G^{uu}(h{=}0) = \int_0^{\infty} \frac{\theta_{xy}}{\sigma_\theta^2} \exp\left(-\frac{\theta_{xy}^2}{\sigma_\theta^2}\right) \sum_{m=0}^{M} \mathcal{H}(m) \left(\frac{\theta_{xy}^2}{\sigma_\theta^2}\right)^m d\theta_{xy} = \sum_{m=0}^{M} \frac{\mathcal{H}(m) m!}{2}. \quad (26)$$

Using [27, Eq. (3.351.3)] and after some mathematical derivations, the closed form expression for (25) is derived as

$$f_G^{uu}(h{>}0) \simeq \sum_{j=0}^{J} \left(\frac{\mathcal{A}_j(\alpha,\beta)}{1+2a_j\sigma_\theta^2} h^{\beta-1+j} \ -\frac{\mathcal{A}_j(\beta,\alpha,)}{1+2b_j\sigma_\theta^2} h^{\alpha-1+j} \right) - \sum_{m=0}^{M} \sum_{j=0}^{J} \frac{\mathcal{H}(m)}{2\sigma_\theta^{2m+2}} \left(\frac{m!\mathcal{A}_j(\alpha,\beta)}{(1+a_j\sigma_\theta^2)^{m+1}} h^{\beta-1+j} - \frac{m!\mathcal{A}_j(\beta,\alpha)}{(1+b_j\sigma_\theta^2)^{m+1}} h^{\alpha-1+j} \right). \quad (27)$$

For low values of h, (27) can be simplified as

$$f_G^{uu}(h{>}0) \simeq \frac{\pi\gamma_{uu}^2 \left(\frac{\alpha\beta}{A_0 h_l}\right)^{\beta} \sin^{-1}((\alpha-\beta)\pi)}{\Gamma(\alpha)\Gamma(\beta)\Gamma(-(\alpha-\beta)+1)| - (\beta-\gamma_{uu}^2)|} \times \left(\frac{1}{1+2a_0\sigma_\theta^2} - \frac{1}{2} \sum_{m=0}^{M} \frac{m!\mathcal{H}(m)}{(1+a_0\sigma_\theta^2)^{m+1}} \right) h^{\beta-1}. \quad (28)$$

Note that, as we will explain later, (28) is valid for relatively low values of h, which means that it suitable for performance analysis at relatively low $\mathcal{P}_{\text{out}}$ or low bit-error-rate.

For the sake of completeness, we have provided in Appendix B the PDF of h for UU link under LN turbulence model, see (49). Also, we have considered in Appendix C the special case where the turbulence effect is negligible; the channel distribution is then given by (58).

B. Ground-to-UAV Channel Model

For the GU link, we take into consideration the deviations in the position and the orientation of the Tx due to building sway, i.e., the RVs x_t, y_t, θ_{tx}, and θ_{ty} [18]. For a typical Tx mounted on a building, θ_{tx} and θ_{ty} are usually very small and can be set to zero [4]. As a result, we consider $\theta_{xy} \simeq 0$. Also, we assume that the variances of Tx position fluctuations in x and y axes are the same and equal to σ_g^2. Then, (12) can be simplified to the Rayleigh distribution, as follows:

$$f_{r_{tr}}(r_{tr}) = \left(r_{tr}/\sigma_{pg}^2\right) \exp\left(-r_{tr}^2/2\sigma_{pg}^2\right), \quad (29)$$

where $\sigma_{pg}^2 = \sigma_p^2 + \sigma_g^2$. According to (7), (29) and (15), the distribution of h' for the GU link is obtained as

$$f_{h'}^{\text{G}}(h') = \frac{2\gamma_{gu}^2(\alpha\beta)^{\frac{\alpha+\beta}{2}}}{\Gamma(\alpha)\Gamma(\beta)(A_0 h_l)^{\gamma_{gu}^2}} h'^{\gamma_{gu}^2-1} \times \int_{h'/A_0 h_l}^{\infty} h_a^{\frac{\alpha+\beta}{2}-1-\gamma_{gu}^2} k_{\alpha-\beta}(2\sqrt{\alpha\beta h_a}) dh_a. \quad (30)$$

where $\gamma_{gu}^2 = \frac{w_{zeq}^2}{4\sigma_{pg}^2}$. Similar to the derivation of (18), the closed form expression for (30) is obtained as

$$f_{h'}^{\text{G}}(h') \simeq \sum_{j=0}^{J'} \left(\mathcal{A}_j^{gu}(\alpha,\beta) h'^{\beta-1+j} - \mathcal{A}_j^{gu}(\beta,\alpha) h'^{\alpha-1+j}\right), \quad (31)$$

where $J' = \lfloor \gamma_{gu}^2 - \alpha \rfloor$ and $\mathcal{A}_j^{gu}(\alpha,\beta)$ is obtained from $\mathcal{A}_j(\alpha,\beta)$ by substituting γ_{gu} instead of γ_{uu}.

For GU link, $\theta_a = \sqrt{\theta_{rx}^2 + \theta_{ry}^2}$, which has a Rayleigh distribution as

$$f_{\theta_a}(\theta_a) = \left(\theta_a/\sigma_\theta^2\right) \times \exp\left(-\theta_a^2/2\sigma_\theta^2\right). \quad (32)$$

According to (43) and (32), the distribution of h_{pa} can now be derived as follows

$$f_{h_{pa}}(h_{pa}) = \left[1 - \exp\left(-\theta_{FOV}^2/2\sigma_\theta^2\right)\right] \delta(h_{pa}-1) + \exp\left(-\theta_{FOV}^2/2\sigma_\theta^2\right) \delta(h_{pa}). \quad (33)$$

Then, from (21), (31) and (33), the distribution of h for GU link can be obtained as

$$f_G^{gu}(h) = f_G^{gu}(h>0) + f_G^{gu}(h{=}0)\delta(h), \quad (34)$$

where

$$f_G^{gu}(h{=}0) = \int_0^{\theta_{FOV}} f_{\theta_a}(\theta_a) d\theta_a = \exp\left(-\theta_{FOV}^2/2\sigma_\theta^2\right), \quad (35)$$

and $f_G^{gu}(h>0)$ is obtained as

$$f_G^{gu}(h>0) = \left[1 - \exp\left(-\theta_{FOV}^2/2\sigma_\theta^2\right)\right] \times \sum_{j=0}^{J'} \left(\mathcal{A}_j^{gu}(\alpha,\beta) h'^{\beta-1+j} \ -\mathcal{A}_j^{gu}(\beta,\alpha) h'^{\alpha-1+j}\right). \quad (36)$$

For low values of h, (36) can be simplified as

$$f_G^{gu}(h>0) = \left[1 - \exp\left(-\theta_{FOV}^2/2\sigma_\theta^2\right)\right] \times \frac{\pi\gamma_{gu}^2 \left(\frac{\alpha\beta}{A_0 h_l}\right)^{\beta} \sin^{-1}((\alpha-\beta)\pi) h^{\beta-1}}{\Gamma(\alpha)\Gamma(\beta)\Gamma(-(\alpha-\beta)+1)| - (\beta-\gamma_{gu}^2)|}. \quad (37)$$

The PDF of h for GU link under LN turbulence is provided in Appendix B, see (53). Moreover, in Appendix C, we have presented the GU link channel model for the case of negligible turbulence.

C. UAV-to-Ground Channel Model

For the UG link, the Rx is fixed and we set θ_{rx} and θ_{ry} to zero, resulting in $\theta_a = \theta_{xy}$. Consequently, we have $F_{\theta_a|\theta_{xy}}(\theta_{FOV}) = F_{\theta_a}(\theta_{FOV}) = \Pi\left(\frac{\theta_{xy}}{\theta_{FOV}}\right)$. Following (12)-(48), $f_{h'|\theta_{xy}}$ for the UG link is similar to the case of the UU link when we replace σ_{pg}^2 by $2\sigma_p^2$ in (48). Based on (21), $f_{h|\theta_{xy}}$ is derived as follows.

$$f_{h|\theta_{xy}}(h) = f_{h'|\theta_{xy}}(h)\Pi\left(\frac{\theta_{xy}}{\theta_{FOV}}\right) + \left[1 - \Pi\left(\frac{\theta_{xy}}{\theta_{FOV}}\right)\right] \delta(h). \quad (38)$$

Then, using (13), (18), (38) and [27, Eq. (3.323.3)], the PDF of h is derived as

$$f_G^{ug}(h) = f_G^{ug}(h>0) + f_G^{ug}(h{=}0)\delta(h), \quad (39)$$

TABLE I
SYSTEM PARAMETERS USED THROUGHOUT SIMULATIONS

Parameter	Setting
Wavelength λ	1550 nm
Responsivity R	0.9
Aperture radius r_a	10 cm
Optical bandwidth B_o	10 nm
Electrical bandwidth B_e	1 GHz
Spectral radiance $N_b(\lambda)$	10^{-3} W/cm^2-m-srad
Scattering coefficient ζ	1 Km^{-1}
SD of UAV position σ_p	20 cm
SD of ground station position σ_g	20 cm
Target SNR Υ_{th}	10 dB

where $f_G^{ug}(h{=}0) = f_G^{ug}(h{=}0)$ and $f_G^{ug}(h>0)$ is obtained as

$$f_G^{ug}(h{>}0) \simeq \sum_{j=0}^{J'} \int_0^{\theta_{FOV}} \frac{\theta_{xy}}{\sigma_\theta^2} \exp\left(-\theta_{xy}^2/2\sigma_\theta^2\right) \times \left(\mathcal{A}_j^{gu}(\alpha,\beta) \exp\left(-a_j'\theta_{xy}^2\right) h^{\beta-1+j} - \mathcal{A}_j^{gu}(\beta,\alpha) \exp\left(-b_j'\theta_{xy}^2\right) h^{\alpha-1+j}\right) d\theta_{xy}$$
$$= \sum_{j=0}^{J'} \left(\frac{\mathcal{A}_j^{gu}(\alpha,\beta)}{1+2a_j'\sigma_\theta^2} \left(1 - e^{-\left(a_j'+1/2\sigma_\theta^2\right)\theta_{FOV}^2}\right) h^{\beta-1+j} - \frac{\mathcal{A}_j^{gu}(\beta,\alpha)}{1+2b_j'\sigma_\theta^2} \left(1 - e^{-\left(b_j'+1/2\sigma_\theta^2\right)\theta_{FOV}^2}\right) h^{\alpha-1+j} \right), \quad (40)$$

where $a_j' = \frac{Z^2}{2\sigma_{pg}^2} + \frac{Z^2\gamma_{gu}^2}{2\sigma_{pg}^2(\beta-\gamma_{gu}^2+j)}$ and $b_j' = \frac{Z^2}{2\sigma_{pg}^2} + \frac{Z^2\gamma_{gu}^2}{2\sigma_{pg}^2(\alpha-\gamma_{gu}^2+j)}$. For low values of h, (40) can be simplified as

$$f_G^{ug}(h{>}0) \simeq \frac{\pi\gamma_{gu}^2 \left(\frac{\alpha\beta}{A_0 h_l}\right)^\beta \sin^{-1}((\alpha-\beta)\pi) h^{\beta-1}}{\Gamma(\alpha)\Gamma(\beta)\Gamma(-(\alpha-\beta)+1)|-(\beta-\gamma_{gu}^2)|} \times \frac{1}{1+2a_0'\sigma_\theta^2} \left(1 - e^{-\left(a_0'+1/2\sigma_\theta^2\right)\theta_{FOV}^2}\right). \quad (41)$$

The PDF of h for UG link under LN turbulence is given in Appendix B. The case of negligible turbulence is also considered in Appendix C.

Notice that the proposed channel models were initially characterized by nine RVs, which makes analytical calculation of the link performance very cumbersome. The proposed closed-form expressions for UU, GU, and UG links allow a significant reduction of the computational complexity.

IV. NUMERICAL RESULTS AND DISCUSSION

Here, we firstly use classical Monte-Carlo simulations in order to verify the accuracy of the proposed expressions. We also investigate the impact of different Tx and Rx parameters and link range on the performance of the three considered links. The system parameters we use for performance evaluation are provided in Table I (SD denotes standard deviation). For the analytical results, we set $M = 64$.

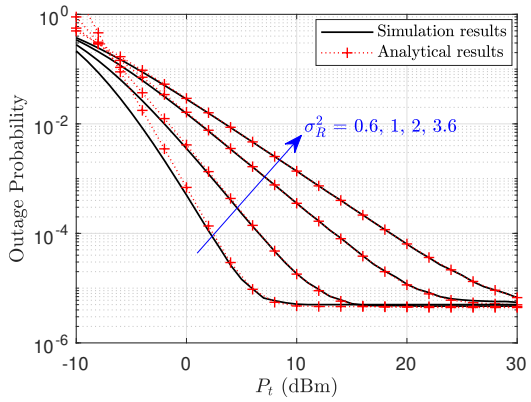

Fig. 4. Outage Probability of the UU link versus P_t over GG turbulence model for $\theta_{FOV} = 7$ mrad, $\sigma_\theta = 1$ mrad, $w_z = 2$ m, $Z = 250$ m and different values of σ_R^2.

Let us first investigate the performance of the considered system under different turbulence conditions. In Fig. 4, we have depicted $\mathcal{P}_{\text{out}}$ of the UU link over GG turbulence for different values of σ_R^2. We firstly notice that, at low values of P_t, as expected, the effect of turbulence on $\mathcal{P}_{\text{out}}$ is very significant. More importantly, regardless of turbulence strength, $\mathcal{P}_{\text{out}}$ is floored at high values of P_t. Indeed, according to (4), h_{th} approaches zero at large P_t. Then, substituting (24) in (3), we have $\mathcal{P}_{\text{out}} \simeq f_h^{uu}(h>0) = \sum_{m=0}^{M} \frac{\mathcal{H}(m)m!}{2}$. According to (46), $\mathcal{H}(m)$ only depends on θ_{FOV} and σ_θ^2, and hence, $\mathcal{P}_{\text{out}}$ does not depend on P_t nor on the turbulence strength. In addition, we notice a perfect match between the analytical and simulation-based results for moderate to strong range of atmospheric turbulence and relatively low $\mathcal{P}_{\text{out}}$ values.

For weak turbulence conditions and relatively high $\mathcal{P}_{\text{out}}$, there is a gap between the analytical and simulation results, which is in fact due to the approximations made in (17). More specifically, according to (7), $f_G(h_a)$ is a function of $k_\varepsilon(\xi)$, where $\varepsilon = \alpha - \beta$ and $\xi = 2\sqrt{\alpha\beta h_a}$. For conventional FSO links, we have typically $4 > \sigma_R^2 > 0.05$ corresponding to $3 > \varepsilon > 1.5$. For this range of ε, (17) is valid approximately for $\xi < 18$. For smaller values of σ_R^2 (weak turbulence), parameters α and β are larger, giving rise to larger h_a, and hence, larger ξ, which compromises the validity of (17).To resolve this problem, we resort to the LN turbulence model for the weak turbulence regime, where our approximations (presented in Appendix B) remain more accurate. For instance, in Figs. 5a-5c, we have presented plots of $\mathcal{P}_{\text{out}}$ as a function of P_t for different values of θ_{FOV} for UU, UG, and GU links for the cases of LN turbulence with $\sigma_{\text{Ln}h_a}^2 = 0.1$ and negligible turbulence. Several important observations can be made from Fig. 5. Firstly, as expected, the UU link has its worst performance in terms of $\mathcal{P}_{\text{out}}$, compared with UG and GU links. Notice that the Rx orientation deviations affect h_{pa} whereas those of Tx affect both h_{pg} and h_{pa}. Also, remember that we have neglected Tx/Rx orientation deviations when they are mounted on a ground station. Consequently, the GU link has a better performance than the UG link. Secondly, at relatively low P_t, smaller values of θ_{FOV} result in a slightly improved performance, which is due to reduced background

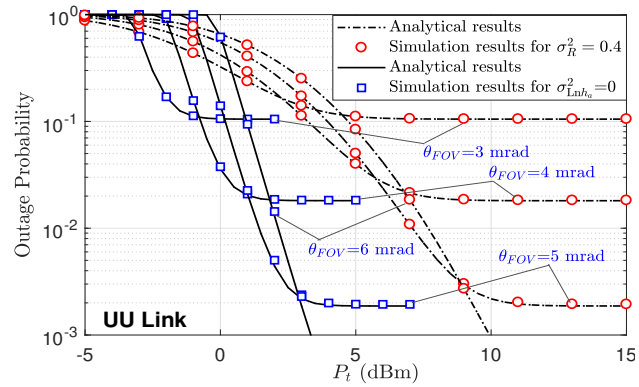

(a)

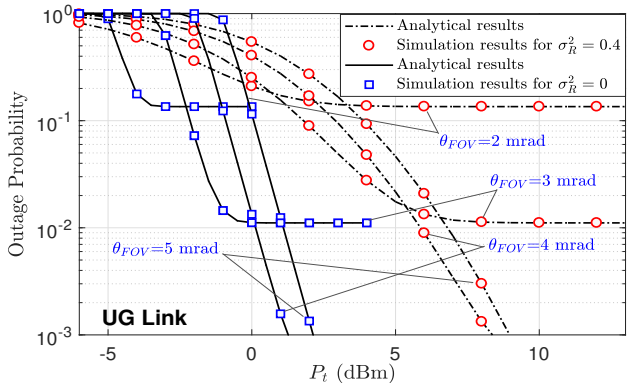

(b)

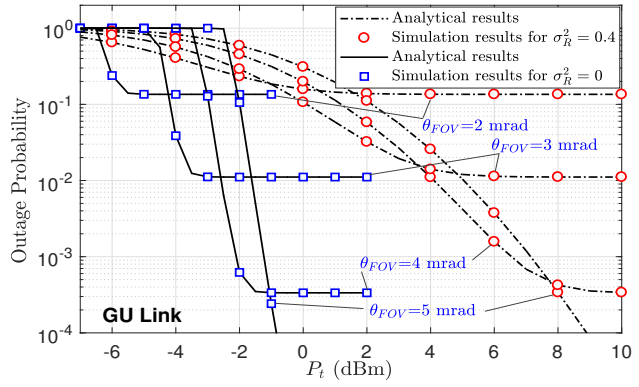

(c)

Fig. 5. Outage probability versus P_t over LN turbulence model for different values of θ_{FOV}. $w_z = 3.5\,\mathrm{m}$, $\sigma_\theta = 1\,\mathrm{mrad}$, $Z = 500\,\mathrm{m}$ and for a) UU, b) UG and c) GU links.

noise level at the Rx. However, for relatively small θ_{FOV}, increased P_t results in a $\mathcal{P}_{out}$ floor. Indeed, as we see from the derivations of Section III, in such situations, $\mathcal{P}_{out}$ just depends on the AOA fluctuations and θ_{FOV}. As we can notice from (49), (26) and (46) for UU link, increasing θ_{FOV} allows a decrease in $\mathcal{P}_{out}$ due to AOA fluctuations. Meanwhile, a larger θ_{FOV} results in an increased background noise level; thus the importance of finding an optimal value for θ_{FOV} to minimize $\mathcal{P}_{out}$ at a given P_t (as we will discuss later). Meanwhile, we again notice the perfect match between simulation and analytical calculation results.

To get more insight into the importance of optimizing w_z and θ_{FOV}, we have presented for the UU link plots of $\mathcal{P}_{out}$ versus a wide range of beam waist and FOV in Figs. (6a) and (6b) for $P_t = 15$ and $25\,\mathrm{dBm}$, respectively. We notice the high sensitivity of the link performance to w_z and θ_{FOV}. Moreover, by increasing P_t the optimum θ_{FOV} and w_z are increased: they are $11.8\,\mathrm{mrad}$ and $3.2\,\mathrm{m}$ for $P_t = 15\,\mathrm{dBm}$, compared to $16.5\,\mathrm{mrad}$ and $3.8\,\mathrm{m}$ for $P_t = 25\,\mathrm{dBm}$. The dependence of the optimum values on P_t suggests that they are also function of the background noise level in practice.

In addition to P_t, other channel parameters such as link range Z and the variance of orientation fluctuations of Tx/Rx σ_θ^2 affect the link performance and consequently, the optimum values of θ_{FOV} and w_z. This is shown in Tables II and III for $P_t = 15\,\mathrm{dBm}$ and different values of Z and σ_θ, respectively. Also, the minimum achievable $\mathcal{P}_{out}$ and the corresponding link interruption probability (due to the AOA fluctuations) are given. We notice from Table II that for a fixed σ_θ, we need a larger θ_{FOV} at shorter Z to minimize $\mathcal{P}_{out}$ which is due to a lower link interruption probability for a given σ_θ. The optimum θ_{FOV} makes a compromise between increased geometric loss and the Rx background noise level on one hand, and the decrease in the link interruption probability on the other hand. However, the change in σ_θ and Z (and hence, in h_l) makes it very difficult to predict the behavior of the optimum w_z. From Table III, we notice that as σ_θ decreases, the optimal θ_{FOV} and w_z decrease. This is reasonable because for smaller pointing errors, we can make the beam more directional to reduce the geometric loss and the Rx background noise at the same time. Reasonably, we obtain a smaller $\mathcal{P}_{out}$ as well.

V. Concluding Remarks and Future Directions

The goal of this paper was to provide an accurate and computationally efficient channel model for the case of MR UAV-based FSO communications. Thanks to the proposed model, we also considered the optimization of the Tx/Rx tunable parameters (such as beam waist and FOV) in order to achieve the best performance, e.g., the lowest outage probability. The optimal parameters highly depend on channel conditions such as range, turbulence strength, payload vibrations, transmit power, and background noise power. The proposed channel model, which takes into account as many as nine random parameters, was shown to be of significantly high accuracy, allowing easy calculation and tuning of optimal Tx/Rx parameters in an adaptive FSO system, thus removing the need to complex and time consuming Monte Carlo simulations.

Lastly, as a future research direction, one can consider deriving closed-form expressions for the tunable parameters (i.e., the Tx beam waist and the Rx FOV). Another direction concerns the more general case of mobile UAVs, whose instantaneous positions are calculated through accurate information exchange between them on speed, acceleration, distance, and movement direction. There, the proposed channel model should be completed by taking into account estimation errors on such parameters.

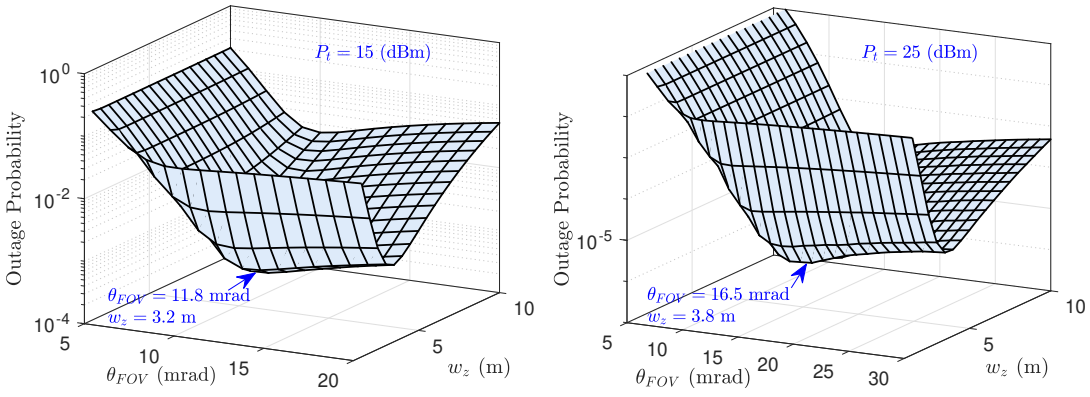

Fig. 6. Outage probability of UU link versus θ_{FOV} and w_z over GG turbulence model for $Z = 500$ m, $\sigma_R^2 = 1$ and a) $P_t = 15$ dBm and b) $P_t = 25$ dBm.

TABLE II
OPTIMUM VALUES OF θ_{FOV} AND w_z TO ACHIEVE MINIMUM OUTAGE PROBABILITY OVER GG TURBULENCE MODEL FOR $\sigma_R^2 = 1$, σ_θ=2 mrad AND P_t=15 dBm AND DIFFERENT VALUES OF Z.

	UAV-to-UAV				UAV-to-Ground				Ground-to-UAV			
Z (km)	θ_{FOV} (mrad)	w_z (m)	$\mathcal{P}_{out}$	$f_h^{uu}(h=0)$	θ_{FOV} (mrad)	w_z (m)	$\mathcal{P}_{out}$	$f_h^{ug}(h=0)$	θ_{FOV} (mrad)	w_z (m)	$\mathcal{P}_{out}$	$f_h^{gu}(h=0)$
0.25	14.3	2.1	1.9×10^{-5}	1.7×10^{-6}	10.7	1.8	3.8×10^{-6}	5.3×10^{-7}	15.4	0.6	6.2×10^{-8}	1.1×10^{-9}
0.5	12.4	3.6	6.4×10^{-4}	5.7×10^{-5}	9.6	3.2	1.4×10^{-4}	1.3×10^{-5}	14.8	0.6	9.4×10^{-8}	2.3×10^{-9}
1	9.9	5.9	0.11	2.2×10^{-2}	7.3	5.4	6.3×10^{-2}	1.4×10^{-2}	13.8	0.5	1.8×10^{-7}	2.6×10^{-8}
1.5	7.8	7.7	0.32	0.1	5.8	6.6	0.12	8.2×10^{-2}	12.7	0.5	7.3×10^{-7}	8.9×10^{-8}

TABLE III
OPTIMUM VALUES OF θ_{FOV} AND w_z TO ACHIEVE MINIMUM OUTAGE PROBABILITY OVER GG TURBULENCE MODEL FOR $\sigma_R^2 = 1$, $Z = 500$ M AND P_t=15 dBm AND DIFFERENT VALUES OF σ_θ.

	UAV-to-UAV				UAV-to-Ground				Ground-to-UAV			
σ_θ (mrad)	θ_{FOV} (mrad)	w_z (m)	$\mathcal{P}_{out}$	$f_h^{uu}(h=0)$	θ_{FOV} (mrad)	w_z (m)	$\mathcal{P}_{out}$	$f_h^{ug}(h=0)$	θ_{FOV} (mrad)	w_z (m)	$\mathcal{P}_{out}$	$f_h^{gu}(h=0)$
8	29.1	5.2	0.16	3.4×10^{-2}	23.4	3.3	5.3×10^{-2}	1.1×10^{-2}	36,2	1.3	2.6×10^{-4}	6.5×10^{-5}
4	21.1	3.3	8.3×10^{-3}	1.1×10^{-3}	16.4	2.8	1.9×10^{-3}	5.4×10^{-4}	19.1	1.4	6.5×10^{-5}	1.1×10^{-5}
2	13.2	2.1	1.7×10^{-4}	2.3×10^{-5}	9.9	1.74	3.6×10^{-5}	6.6×10^{-6}	10.1	1.6	1.6×10^{-5}	3.6×10^{-6}
1	7.4	1.1	4.3×10^{-6}	1.5×10^{-6}	5.5	1.4	3.2×10^{-6}	3.4×10^{-7}	5.6	1.7	8.8×10^{-7}	2.1×10^{-7}

APPENDIX A
DERIVATION OF EQ. (21)

According to Eq. (19), the RV θ_a conditioned on θ_{tx} and θ_{ty} has a Rician distribution expressed as

$$f_{\theta_a|\theta_{xy}}(\theta_a) = \frac{\theta_a}{\sigma_\theta^2}\exp\left(-\frac{\theta_a^2+\theta_{xy}^2}{2\sigma_\theta^2}\right) I_0\left(\frac{\theta_a\theta_{xy}}{\sigma_\theta^2}\right). \quad (42)$$

From (42) and (20), the distribution of h_{pa} can be derived as

$$f_{h_{pa}|\theta_{xy}}(h_{pa}) = F_{\theta_a|\theta_{xy}}(\theta_{FOV})\delta(h_{pa}-1) + \left(1-F_{\theta_a|\theta_{xy}}(\theta_{FOV})\right)\delta(h_{pa}), \quad (43)$$

where

$$F_{\theta_a|\theta_{xy}}(\theta_{FOV}) = \int_0^{\theta_{FOV}} f_{\theta_a|\theta_{xy}}(\theta_a)d\theta_a. \quad (44)$$

Using the polynomial approximation for $I_k(x)$ from [28, Eq. (19)] and [29, Eq. (6)], a closed-form expression for (44) can be derived as

$$F_{\theta_a|\theta_{xy}}(\theta_{FOV}) \simeq 1-\exp\left(-\frac{\theta_{xy}^2}{2\sigma_\theta^2}\right)\sum_{m=0}^{M}\mathcal{H}(m)\left(\frac{\theta_{xy}^2}{\sigma_\theta^2}\right)^m, \quad (45)$$

where

$$\mathcal{H}(m) = \frac{2^{-m}M^{(1-2m)}\Gamma(M+m)\Gamma\left(m+1,\frac{\theta_{FOV}^2}{2\sigma_\theta^2}\right)}{\left(\Gamma(m+1)\right)^2\Gamma(M-m+1)}, \quad (46)$$

and $\Gamma(.,.)$ denotes upper incomplete gamma function [27]. Note that, when $M\to\infty$, Equation (45) degenerates into (44) [27]. Since $h = h_{pa}h'$ and the RVs h_{pa} and h' are independent conditioned on θ_{xy}, the distribution of RV h conditioned on θ_{xy} can be obtained as

$$\begin{aligned} f_{h|\theta_{xy}}(h) &= \int_0^\infty f_{h|h',\theta_{xy}}(h) f_{h'|\theta_{xy}}(h')dh' \\ &= \int_0^\infty \frac{1}{h'} f_{h_{pa}|\theta_{xy}}\left(\frac{h}{h'}\right) f_{h'|\theta_{xy}}(h')dh' \\ &= \int_0^\infty \frac{f_{h'|\theta_{xy}}(h')}{h'}\left[F_{\theta_a|\theta_{xy}}(\theta_{FOV})\delta\left(\frac{h-h'}{h'}\right) \right. \\ &\quad \left. + \left(1-F_{\theta_a|\theta_{xy}}(\theta_{FOV})\right)\delta\left(\frac{h}{h'}\right)\right]dh' \end{aligned}$$

$$f_L^{uu}(h{>}0) = C_a h^{\gamma_{uu}^2-1}\int_0^\infty \frac{\theta_{xy}}{\sigma_\theta^2}\left(1-\exp\left(-\theta_{xy}^2/2\sigma_\theta^2\right)\sum_{m=0}^{M}\mathcal{H}(m)\left(\theta_{xy}^2/\sigma_\theta^2\right)^m\right) \times \exp\left[\left(Z^2/2\sigma_p^2-1/2\sigma_\theta^2\right)\theta_{xy}^2\right] Q\left(\left(w_{z_{eq}}^2\ln\left(h/A_0h_l\right)+6Z^2\theta_{xy}^2+C_b\right)\Big/\sqrt{32\sigma_p^2Z^2\theta_{xy}^2+C_c}\right) d\theta_{xy}. \quad (50)$$

$$\begin{aligned} &= \int_0^\infty f_{h'|\theta_{xy}}(h')\Big[F_{\theta_a|\theta_{xy}}(\theta_{FOV})\delta\left(h-h'\right) \\ &\quad + \left(1-F_{\theta_a|\theta_{xy}}(\theta_{FOV})\right)\delta\left(h\right)\Big]dh' \\ &= F_{\theta_a|\theta_{xy}}(\theta_{FOV})f_{h'|\theta_{xy}}(h) \\ &\quad + \left(1-F_{\theta_a|\theta_{xy}}(\theta_{FOV})\right)\delta(h). \end{aligned} \quad (47)$$

Appendix B
Derivations of Channel Distribution Over Log-Normal Turbulence Model

1) UAV-to-UAV Channel Modeling: Substituting (6), (13) and (14) in (15) and using [4, Eqs. (9), (10)], the distribution of $h' = h_l h_a h_{pg}$ conditioned on θ_{xy} is obtained as

$$f_{h'|\theta_{xy}}^{\mathrm{L}}(h') = C_a h'^{\gamma_{uu}^2-1}\exp\left(Z^2\theta_{xy}^2/2\sigma_p^2\right) \times Q\left(\frac{w_{z_{eq}}^2\ln\left(h'/A_0h_l\right)+6Z^2\theta_{xy}^2+C_b}{\sqrt{32\sigma_p^2Z^2\theta_{xy}^2+C_c}}\right), \quad (48)$$

where $C_a = \gamma_{uu}^2/\left(A_0h_l\right)^{\gamma_{uu}^2} \times \exp\left(2\sigma_{Lnh_a}^2\gamma_{uu}^2(1+\gamma_{uu}^2)\right)$, $C_b = 2\sigma_{Lnh_a}^2 w_{z_{eq}}^2(1+2\gamma_{uu}^2)$, $C_c = 4\sigma_{Lnh_a}^2 w_{z_{eq}}^4$ and $Q(.)$ is the well-known Q-function. Substituting (13), (48), (21) and (22) in (23), we obtain the PDF of h for UU link as

$$f_L^{uu}(h) = f_L^{uu}(h>0) + f_L^{uu}(h=0)\delta(h), \quad (49)$$

where $f_L^{uu}(h=0) = f_G^{uu}(h=0)$ and $f_L^{uu}(h>0)$ is expressed in (50).

2) Ground-to-UAV Channel Modeling: Using (29) and [18, Eqs, (10), (11), (14)], the distribution of h' for the GU link is obtained as

$$f_{h'}^{\mathrm{L}},(h') = C_e h'^{(\gamma_{gu}^2-1)}Q\left(\frac{\ln\left(h'/A_0h_l\right)+C_d}{2\sigma_{\mathrm{Ln}h_a}}\right), \quad (51)$$

where $C_e = \frac{\gamma_{gu}^2}{\left(A_0h_l\right)^{\gamma_{gu}^2}}\exp\left(2\sigma_{\mathrm{Ln}h_a}^2\gamma_{gu}^2(1+\gamma_{gu}^2)\right)$, and $C_d = 2\sigma_{\mathrm{Ln}h_a}^2(1+2\gamma_{gu}^2)$. From (21), (51) and (33), the distribution of h for GU link can be obtained as

$$f_L^{gu}(h) = f_L^{gu}(h>0) + f_L^{gu}(h{=}0)\delta(h), \quad (52)$$

where $f_L^{gu}(h{=}0) = f_G^{gu}(h{=}0)$ and $f_L^{gu}(h>0)$ is obtained as

$$f_L^{gu}(h>0) = C_e\left[1-\exp\left(-\theta_{FOV}^2/2\sigma_\theta^2\right)\right]h^{(\gamma_{gu}^2-1)} \times Q\left(\left(\ln\left(\frac{h}{A_0h_l}\right)+C_d\right)\Big/2\sigma_{\mathrm{Ln}h_a}\right). \quad (53)$$

3) UAV-to-Ground Channel Modeling: Using (13), (48) and (38), the PDF of h for UG link is obtained as

$$f_L^{ug}(h) = f_L^{ug}(h>0) + f_L^{ug}(h{=}0)\delta(h), \quad (54)$$

where $f_L^{ug}(h{=}0){=}f_L^{gu}(h{=}0)$ and $f_L^{ug}(h>0)$ is given in (55).

Appendix C
Derivations of Channel Distribution in the Absence of Atmospheric Turbulence

Here, we consider the special case where the atmospheric turbulence has a negligible effect, i.e., $h' = h_l h_{pg}$.

1) For UU Link: Under such condition, distribution of h conditioned on θ_{xy} can be simplified as

$$f_{h'|\theta_{xy}}(h) = \frac{1}{h_l}f_{h_{pg}|\theta_{xy}}(h'/h_l), \quad \text{for} \quad 0\le h'\le A_0h_l. \quad (56)$$

Now, by substituting (56) in (22), we have

$$f_{h|\theta_{xy}}(h) = \frac{1}{h_l}F_{\theta_a|\theta_{xy}}(\theta_{FOV})f_{h_{pg}|\theta_{xy}}(h/h_l) + \left(1-F_{\theta_a|\theta_{xy}}(\theta_{FOV})\right)\delta(h), \quad \text{for} \quad 0\le h\le A_0h_l. \quad (57)$$

According to (23) and (57) and also using [27, Eq. (8.445)] and [27, Eq. (3.381.4)], after some algebra, (49) is simplified as

$$f_h^{uu,l}(h) = \left(\frac{h}{A_0h_l}\right)^{\gamma^2-1}\sum_{k=0}^{\infty}F(k)\left(\ln\left(\frac{h}{A_0h_l}\right)\right)^k + \sum_{m=0}^{M}\frac{\mathcal{H}(m)m!}{2}, \quad \text{for} \quad 0\le h\le A_0h_l, \quad (58)$$

where, for a given k, $F(k)$ is a constant and is obtained as

$$F(k) = \frac{\gamma^2}{2h_lA_0\sigma_\theta^2}\frac{1}{(k!)^2}\left(-\frac{Z^2\gamma^2}{4\sigma_p^2}\right)^k\left\{\frac{\Gamma(k+1)}{\left(\frac{Z^2}{4\sigma_p^2}+\frac{1}{2\sigma_\theta^2}\right)^{k+1}} - \sum_{m=0}^{M}\frac{\mathcal{H}(m)\Gamma(k+m+1)}{\left(\frac{Z^2}{4\sigma_p^2}+\frac{1}{\sigma_\theta^2}\right)^{k+1}\left(\frac{Z^2\sigma_\theta^2}{4\sigma_p^2}+1\right)^m}\right\}. \quad (59)$$

2) For UG Link: At this condition, the distribution of RV h' conditioned on θ_{xy} can be obtained as (57) and the distribution of h for UG link can be simplified as

$$f_h^{ug,l}(h) = \int_0^{\theta_{FOV}}\frac{\gamma_{gu}^2}{h_lA_0}\exp\left(-\frac{\theta_{xy}^2Z^2}{2\sigma_{pg}^2}\right)\left(\frac{h}{h_lA_0}\right)^{\gamma_{gu}^2-1} \times I_0\left(Z\theta_{xy}\sqrt{-\frac{2\gamma_{gu}^2}{\sigma_{pg}^2}\ln\left(\frac{h}{h_lA_0}\right)}\right)\frac{\theta_{xy}}{\sigma_\theta^2}\exp\left(-\frac{\theta_{xy}^2}{2\sigma_\theta^2}\right)d\theta_{xy} + \exp\left(-\theta_{FOV}^2/2\sigma_\theta^2\right)\delta(h), \quad \text{for} \quad 0\le h\le A_0h_l. \quad (60)$$

According to [27, Eq. (8.445)] and [27, Eq. (3.381.2)] and after some manipulation, we have

$$f_h^{ug,l}(h) = \left(\frac{h}{h_lA_0}\right)^{\gamma_{gu}^2-1}\sum_{k=1}^{\infty}F_{ug}(k)\left(-\ln\left(\frac{h}{h_lA_0}\right)\right)^k + \exp\left(-\theta_{FOV}^2/2\sigma_\theta^2\right)\delta(h), \quad \text{for} \quad 0\le h\le A_0h_l. \quad (61)$$

$$f_L^{ug}(h{>}0) = C_a h^{\gamma_{gu}^2-1} \int_0^{\theta_{FOV}} \frac{\theta_{xy}}{\sigma_\theta^2} \exp\left[\left(\frac{Z^2}{\sigma_{pg}^2} - \frac{1}{2\sigma_\theta^2}\right)\theta_{xy}^2\right] Q\left(\frac{w_{z_{eq}}^2 \ln\left(h/A_0 h_l\right) + 6Z^2\theta_{xy}^2 + C_b}{\sqrt{16\sigma_{pg}^2 Z^2 \theta_{xy}^2 + C_c}}\right) d\theta_{xy}. \quad (55)$$

where, for a given k, $F_{ug}(k)$ is a constant and is obtained as

$$F_{ug}(k) = \frac{\gamma_{gu}^2}{h_l A_0 \sigma_\theta^2} \left(Z^2\gamma_{gu}^2/2\sigma_{pg}^2\right)^k \times \sum_{n=1}^{\infty} \frac{\left(\theta_{FOV}\right)^{n+k+1}}{n!(k+n+1)} \left[-\left(\frac{Z^2}{2\sigma_{pg}^2} + \frac{1}{2\sigma_\theta^2}\right)\right]^n. \quad (62)$$

3) For GU Link: Similar to our previous derivations, the distribution of h in the GU link can be expressed as

$$f_h^{gu,l} = \left[1 - \exp\left(-\theta_{FOV}^2/2\sigma_\theta^2\right)\right] \left(\gamma_{gu}^2/A_0^{\gamma_{gu}^2}\right) h^{\gamma_{gu}^2-1} + \exp\left(-\theta_{FOV}^2/2\sigma_\theta^2\right) \delta(h). \quad (63)$$

REFERENCES

[1] M. A. Khalighi and M. Uysal, "Survey on free space optical communication: A communication theory perspective," *IEEE Commun. Surv. Tutorials*, vol. 16, no. 4, pp. 2231–2258, 2014.

[2] Z. Ghassemlooy, W. Popoola, and S. Rajbhandari, *Optical wireless communications*. CRC Press Boca Raton, FL, 2012.

[3] D. Schulz, V. Jungnickel, C. Alexakis, M. Schlosser, J. Hilt, A. Paraskevopoulos, L. Grobe, P. Farkas, and R. Freund, "Robust optical wireless link for the backhaul and fronthaul of small radio cells," *J. Lightw. Technol.*, vol. 34, no. 6, pp. 1523–1532, 2016.

[4] F. Yang, J. Cheng, and T. A. Tsiftsis, "Free-space optical communication with nonzero boresight pointing errors," *IEEE Trans. Commun.*, vol. 62, no. 2, pp. 713–725, 2014.

[5] B. Zhu, J. Cheng, M.-S. Alouini, and L. Wu, "Relay placement for FSO multihop DF systems with link obstacles and infeasible regions," *IEEE Trans. Wireless Commun.*, vol. 14, no. 9, pp. 5240–5250, 2015.

[6] L. Li *et al.*, "80-Gbit/s 100-m free-space optical data transmission link via a flying UAV using multiplexing of orbital-angular-momentum beams," *arXiv preprint arXiv:1708.02923*, 2017.

[7] G. A. Cap, H. H. Refei, and J. J. Sluss, "Optical tracking and auto-alignment transceiver system," *IEEE Aerosp. Electron. Syst. Mag.*, vol. 25, no. 9, pp. 26–34, 2010.

[8] B. Moision *et al.*, "Demonstration of free-space optical communication for long-range data links between balloons on Project Loon," in *Proc. of SPIE Vol*, vol. 10096, 2017, pp. 100 960Z–1.

[9] C. Chen *et al.*, "High-speed optical links for UAV applications," vol. 10096, pp. 1 009 615–1, 2017.

[10] H. Kaushal and G. Kaddoum, "Optical communication in space: Challenges and mitigation techniques," *IEEE Commun. Surveys Tuts.*, vol. 19, no. 1, pp. 57–96, 2017.

[11] E. Kalantari, M. Z. Shakir, H. Yanikomeroglu, and A. Yongacoglu, "Backhaul-aware robust 3D drone placement in 5G+ wireless networks," in *2017 IEEE Int. Conf. Commun. (ICC),*. IEEE, 2017, pp. 109–114.

[12] A. Kaadan, H. H. Refai, and P. G. LoPresti, "Multielement FSO transceivers alignment for inter-UAV communications," *J. Lightw. Technol.*, vol. 32, no. 24, pp. 4183–4193, 2014.

[13] M. Alzenad, M. Z. Shakir, H. Yanikomeroglu, and M.-S. Alouini, "FSO-based vertical backhaul/fronthaul framework for 5G+ wireless networks," *IEEE Commun. Mag.*, vol. 56, no. 1, pp. 218–224, 2018.

[14] W. Fawaz, C. Abou-Rjeily, and C. Assi, "UAV-Aided Cooperation for FSO Communication Systems," *IEEE Commun. Mag.*, vol. 56, no. 1, pp. 70–75, 2018.

[15] P. J. Cruz and R. Fierro, "Towards optical wireless communications between micro unmanned aerial and ground systems," pp. 669–676, 2015.

[16] M. Khan, M. Yuksel, and G. Winkelmaier, "GPS-free maintenance of a free-space-optical link between two autonomous mobiles," *IEEE Trans. Mobile Comput.*, vol. 16, no. 6, pp. 1644–1657, 2017.

[17] A. Kaadan, H. Refai, and P. Lopresti, "Spherical FSO receivers for UAV communication: geometric coverage models," *IEEE Trans. Aerosp. Electron. Syst.*, vol. 52, no. 5, pp. 2157–2167, 2016.

[18] A. A. Farid and S. Hranilovic, "Outage capacity optimization for free-space optical links with pointing errors," *J. Light. Technol.*, vol. 25, no. 7, pp. 1702–1710, 2007.

[19] S. Huang and M. Safari, "Free-space optical communication impaired by angular fluctuations," *IEEE Trans. Wireless Commun.*, 2017.

[20] M. A. Khalighi, F. Xu, Y. Jaafar, and S. Bourennane, "Double-laser differential signaling for reducing the effect of background radiation in free-space optical systems," *IEEE/OSA J. Opt. Commun. Net.*, vol. 3, no. 2, pp. 145–154, Feb. 2011.

[21] F. Xu, M. A. Khalighi, and S. Bourennane, "Impact of different noise sources on the performance of PIN- and APD-based FSO receivers," *IEEE ConTEL Conf.*, pp. 211–218, June 2011, Graz, Austria.

[22] M. T. Dabiri, S. M. S. Sadough, and M. A. Khalighi, "FSO channel estimation for OOK modulation with APD receiver over atmospheric turbulence and pointing errors," *Opt. Commun.*, vol. 402, pp. 577–584, 2017.

[23] N. S. Kopeika and J. Bordogna, "Background noise in optical communication systems," *Proceedings of the IEEE*, vol. 58, no. 10, pp. 1571–1577, 1970.

[24] L. C. Andrews and R. L. Phillips, *Laser beam propagation through random media*. SPIE press Bellingham, WA, 2005, vol. 52.

[25] M.-A. Khalighi, N. Schwartz, N. Aitamer, and S. Bourennane, "Fading reduction by aperture averaging and spatial diversity in optical wireless systems," *J. opt. commun. netw.*, vol. 1, no. 6, pp. 580–593, 2009.

[26] Wolfram, "The wolfram functions site: http://functions.wolfram.com/," 2001.

[27] I. S. Gradshteyn and I. M. Ryzhik, *Table of integrals, series, and products*. 7th ed. Academic press, 2007.

[28] L. Li, F. Li, and F. Gross, "A new polynomial approximation for J ν Bessel functions," *Applied mathematics and computation*, vol. 183, no. 2, pp. 1220–1225, 2006.

[29] P. C. Sofotasios and S. Freear, "Novel expressions for the Marcum and one dimensional Q-functions," pp. 736–740, 2010.